

# A NEW TWO-FLARE-SHAPED UWB ANTENNA ELEMENT

Anatoliy O. Boryssenko<sup>1)</sup>, Dmitriy L. Sostanovsky<sup>2)</sup>

<sup>1)</sup>Antennas & Propagation Laboratory, University of Massachusetts, Amherst

<sup>2)</sup>Ratio Research Company, Kiev, Ukraine

## Abstract

**A novel compact UWB antenna is based on using of two smoothly shaped flares of a simple geometrical structure. The first flare, larger in size, serves as an antenna base, reflector and one of the radiator arms. The second flare, smaller in size, operates as the other arm of the radiator. An apparent idea is exploited in this design that an “ideal” UWB antenna would operate as a broadband well-matched transformer for the current at its driving ports to the radiated fields that leave the antenna aperture. Besides terminal matching, the antenna would provide a necessary spatial distribution of the radiated energy. In order to create such a current-to-field transformer the flares of the proposed antenna are properly shaped and driven through direct connection to coaxial cables without balun. The antenna is studied through numerical full-wave simulations and tests with several prototypes. The achieved performance in the band  $>5:1$  involves  $<-10\text{dB}$  return loss,  $>10\text{dB}$  front-to-back ratio, constant  $>5$  dBi directive gain, constant beamwidth, and suitability for pulse transmission with minimized distortions.**

## 1. Antennas for UWB Systems

Previously and in the coming years, there is a great interest in short range high-speed data transmissions, high-resolution sensing and ranging using the Ultra-Wideband (UWB) technology [1-3]. Unlike traditional narrowband systems, their UWB counterparts operate by employing very short electrical pulses of nanosecond and subnanosecond duration resulting in very wide transmission bandwidths ranging from several hundred megahertz up to several gigahertz. Such huge bandwidths must be supported with suitable UWB antennas that behave unavoidably as bandpass filters [4,5].

As a result, UWB antennas must be properly designed to enhance the potential advantages of short-pulse signaling for communication, ranging, sensing and other applications. For many applications, minimal pulse distortion is the primary focus because useful information may be contained in the signal shape or precise timing of the signaling pulses. Minimized pulse distortion is equivalent to supporting clean well-confined impulse responses in time-domain or “flat gain” and “linear phase” for frequency domain transfer functions [4]. Both of these quantities collect the key electrical

features of individual antennas such as: (1) input impedance bandwidth and (2) radiation features (directive gain, pattern shapes, beamwidth, front-to-back ratio, etc.).

UWB antenna designer may chose among known antenna solutions or create new ones to meet diverse system-related requirements, electrical, mechanical, manufacturing and cost constraints. Some authors considered historically an ideal UWB antenna that radiates time derivatives of the input signal [6] but this principle is not helpful to design practical UWB radiators. Rather other rational and physics-based guidelines could be more productive [7].

The presented antenna has been developed to provide a well-behaved radiator operating as a single element and/or array element in UWB time-domain radar and telecommunication systems. Specifically, the antenna must meet the following key functional demands: (1) broadband impedance matching to the 50  $\Omega$ ; (2) direct coaxial cable feeding without balun; (3) minimized distortions for pulse transmission, (4) good radiation features to provide well-confined beams with minimum front-to-back ratio; (5) simplicity and compactness of geometrical shape, (6) suitability for easy prototyping and manufacturing at a reduced cost.

Reviewing the UWB antenna related literature [7-13] leads to a conclusion that neither of such known radiators like those schematically sketched in Figure 1 can meet the above demands. In general, the impedance bandwidth is better supported in protruded antennas like TEM horn, tapered slot and log-periodic. The log-periodic dipole array is back-fire antenna and is highly dispersive. Directive radiation patterns are provided by using apertures of larger extent and/or backside reflectors, e.g. in impulse radiating antenna that is large. Furthermore, the use of a reflector to improve front-to-back ratio degrades impedance bandwidth, e.g. a broadband dipole over a ground plane. Also, the most of the antennas in Figure 1 excepting the trapezoidal one [9,10] are balance-fed structures that require balun for feeding through coaxial lines. As a rule, balun has limited bandwidth that impacts additionally on the whole achievable bandwidth.

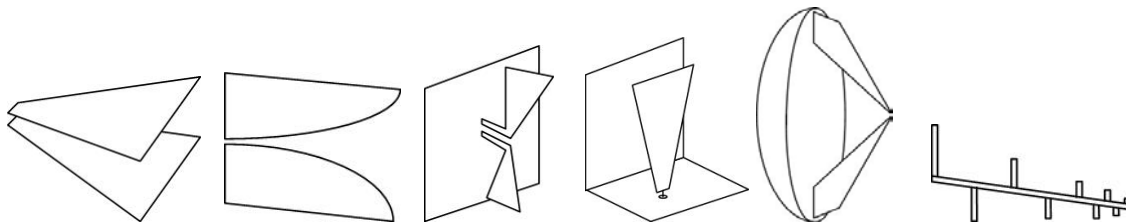


**Figure 1.** Sketches of canonical antenna shapes (from the left to the right): TEM-horn, tapered-slot (Vivaldi), dipole with backside reflector, trapezoidal antenna, impulse radiating antenna (reflector with feeding TEM-horn), log-periodic dipole array.

## 2. Novel UWB Antenna Design Concept

This work deals with a new type of UWB directive low-dispersion antenna [14] that has some superior characteristics with respect to other known UWB radiators. A simplified geometrical sketch of this antenna is in Figure 2a and its first prototype made in Kiev in 2003 is pictured in Figure 2 b-c. The antenna radiates in its broadside direction, normal to its aperture. It is linearly-polarized, similar to that for the TEM horn, with the same flare orientation but with more efficient using of physical space when providing comparable terminal and radiation characteristics.

As a matter of fact, an old and well-known idea, see e.g. [7], is exploited in the antenna design. This idea states that a well-behaved radiator must act as a well-matched transformer from the current at its driving port to the radiated fields leaving the antenna aperture and providing necessary distribution of the radiated energy in space. Such a current-to-field transformer is created by two smoothly shaped metal flares of the proper geometrical configuration. In particular, the first flare, larger in size, is called the “reflector”, Figure 2a. It serves simultaneously as an antenna base, its backside reflector and one of the radiator arms of an asymmetrical TEM-horn-like radiator. The second flare, smaller in size, is called the “tongue”, Figure 2a, and operates as second arm of the radiator. The antenna feeding network is demonstrated in Figure 2c where the 50- $\Omega$  UHF coax connector is mounted from its backside, connected by its ground contact to the reflector and by the central pin to the tongue.

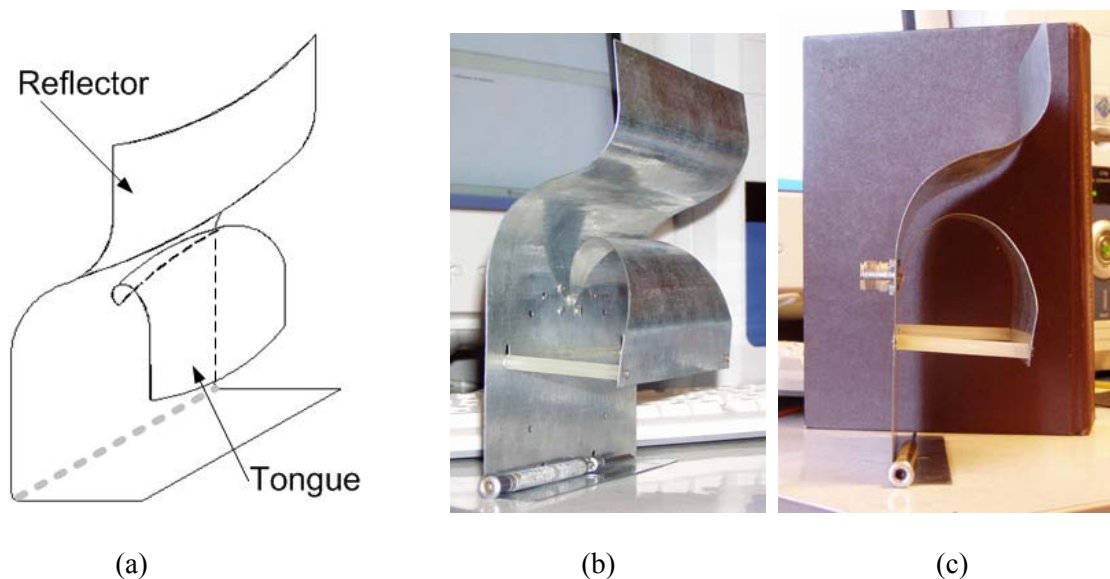


**Figure 2.** Two-flare UWB antenna design: (a) geometrical sketch; (b)-(c) aluminum prototype shown from two observation angles.

By its topology, the proposed design is somewhat similar to a monopole with the angled reflector originated from suspended microstrip patches [12,13] and/or trapezoidal-like antennas [9,10] sketched in Figure 1. Like these earlier antennas, the proposed antenna does not need a separate balun to be fed, e.g. from a 50- $\Omega$  coaxial cable. However, this new design concept differs from its counterparts, viz. suspended patch and trapezoidal antenna, because the bent profiles of the flares enhance its bandwidth and radiation characteristics, which cannot be obtained at an equivalent level with just flat flare surfaces. Comparing to other antenna geometries like that in Figure 1 the present design is also relatively simple and suitable for quite easy prototyping and manufacturing.

Other designs of the two-flare UWB antenna, such are sketched in Figure 3, have been tested with good results. In particular, an antenna with symmetrical reflector and long-base tongue radiator is in Figure 3a. The purpose of such a design modification is (1) increasing its bandwidth through improved impedance matching at the lower frequencies and (2) making more symmetrical the E-plane radiation pattern. A sample of this antenna is presented in the paper with some measured data. Figure 3b provides a sketch of the UWB two-flare antenna that has (1) balanced-fed driver required for some specific applications and (2) improved symmetry of the E-plane radiation pattern compared to the geometry in Figure 3a. Other design modifications are possible including supporting linear dual-polarized operation, reducing the antenna height (broadside extent) by dielectric filling, etc, that are beyond the scope of the paper.

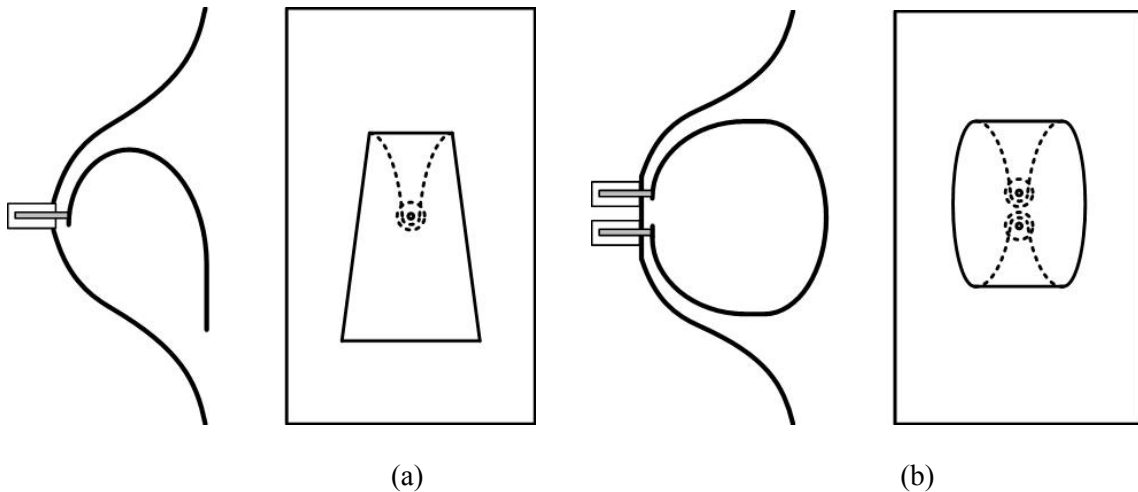


**Figure 3.** Design modification of the two-flare antenna demonstrated with two perspective drawings: (a) Symmetrical reflector and long-base tongue radiator; (b) Balanced-fed two-flare antenna. Coaxial connectors are from the antenna backside.

### 3. Mathematical Model of Antenna Flares' Geometry

Historically, the flare shapes similar to that in Figure 2a are intuitively found through experiments with several original prototypes. Such prototypes can be easily made by cutting and bending soft aluminum or brass sheets. However, a rigorous mathematical description of the flares' shapes is desirable. In general, such a shape can be quantified by means of some geometrical CAD techniques [15] like Bezier curves, NURBS, etc. However, rigorous mathematical description with fewer parameters makes it easier to manipulate the model for parametric analysis and shape optimization, as well as describing the antenna for manufacturing. As a result of several iterations, the “double” exponential model was found to be suited for this purpose. This model is described hereafter in this Section of the paper.

The 3-D geometry of the tongue can be simplified by considering, firstly, the 2-D flare shape, Figure 4, and, secondly, the tongue width profile, Figure 5. The width of the reflector is assumed constant, like those in Figure 2 and 3. The 2-D model of the flare shapes in Figure 3 involves three basic curves # 0, 1 & 2. The curve # 0 is the base for both the flare-shaping curves # 1 & 2 that define the shapes of the reflector and radiator, correspondingly. As an implicit expression  $F^0(x, y)$  for the curve # 0 a so-called “super-ellipse” [16] is used

$$F^0(x, y) = 0 \Leftrightarrow \left(\frac{x-a}{a}\right)^n + \left(\frac{y-b}{b}\right)^n = 1, \quad 0 \leq x \leq a \quad 0 \leq y \leq b \quad (1)$$

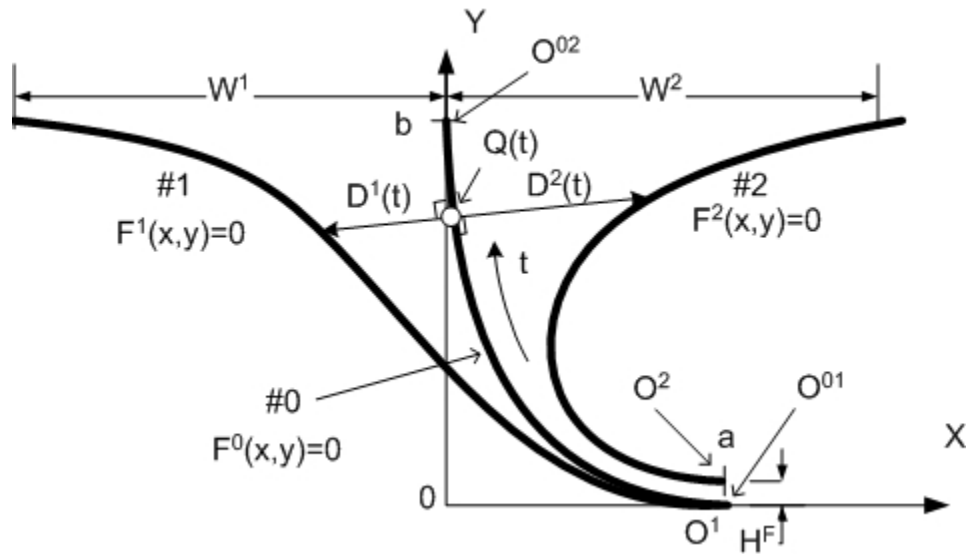


**Figure 4.** Mathematical model of flares based on three curves # 0, 1 & 2 and “double” exponential tapering for the distance between the base curve #0 and flare curves # 1 & 2.

Other shaping functions instead of (1) are possible including exponential function, splines and so on. An arbitrary power factor  $n$  ( $n > 2$ ) is used in (1) to enable flexible shaping for the flares # 1 & 2. The curve #0 is parameterized by the parameter  $t$  that measures its curved length with respect to its endpoint  $O^{01}$ . When the parameter  $t$  reaches endpoint  $O^{02}$  the total length  $T$  of the curve #0 is obtained. Note the parameter  $b$  of the basic shape #0 defines the antenna overall extent (height) along its broadside direction.

The flare shapes given by curves # 1 & 2 are defined by their own implicit expressions  $F^1(x, y)$  and  $F^2(x, y)$  derived through the following mapping procedure. Both the curves start to evolve from their origins, viz.  $O^1$  and  $O^2$ , while obtaining their maximum extents  $W^1$  and  $W^2$ , correspondingly, Figure 4. The quantities  $W^1$  and  $W^2$  present collectively the overall aperture size of the two-flare antenna. The vertical shift between the origin points  $O^1$  and  $O^2$  introduces another important design parameter  $H_F$ , viz. the distance between two flares at the feed point. Typically  $H_F$  is relatively small and equal approximately to the diameter of the coaxial connector used to feed the antennas.

The curves # 1 and 2 are computed versus the parameter  $t$  that is gradually changed with a given increment. Each value of  $t$  defines a point  $Q(t)$  on the curve # 0. Two normal segments can be drawn at each point  $Q(t)$  along the curve # 0. The first normal segment is directed towards the left in Figure 4. It has the length  $D^1(t)$  that defines the reflector-forming curve # 1. The second normal segment is taken towards the right in Figure 4 and has the length  $D^2(t)$  to define a point at the tongue-shaping curve # 2.

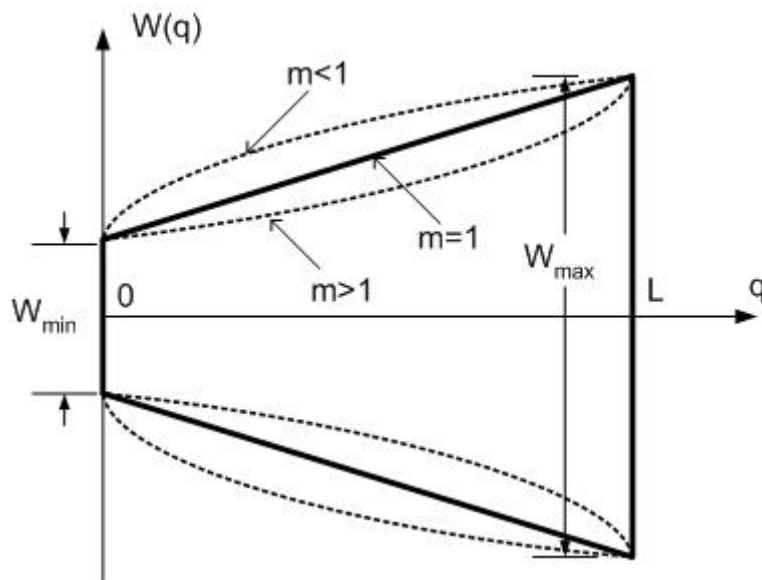


**Figure 5.** Shape generation algorithm for the tongue flare width.

The shaping functions  $F^1(x, y)$  and  $F^2(x, y)$  can be implicitly defined through  $D^1(t)$  and  $D^2(t)$  parametric functions. The later dependencies can be expressed through the exponential shape approximation model that was previously developed to model tapered slots in Vivaldi antenna [17]

$$F^i(x, y) = 0 \Leftrightarrow D^i(t) = C_1^i \cdot \exp\{R^i t\} + C_2^i, \quad i = 1, 2 \quad (2)$$

where the factors  $C_1^i$  and  $C_2^i$  are derived with respect to the minimum  $D_1^i$  ( $t \equiv t_1 = 0$ ) and maximum  $D_2^i$  ( $t \equiv t_2 = T$ ) extent of each flare

$$C_1^i = \frac{D_2^i - D_1^i}{\exp\{R^i t_2\} - \exp\{R^i t_1\}} \quad (3)$$

$$C_2^i = \frac{D_2^i \cdot \exp\{R^i t_2\} - D_1^i \cdot \exp\{R^i t_1\}}{\exp\{R^i t_2\} - \exp\{R^i t_1\}}$$

In particular, one can derive for the geometrical arrangement in Figure 4

$$\begin{aligned} D_1^1 &= D^1(0) = 0 & D_2^1 &= D^1(T) = W^1 \\ D_2^1 &= D^2(0) = H_F & D_2^2 &= D^2(T) = W^2 \end{aligned} \quad (4)$$

The flare approximating function (2)-(3) seems plays a very constructive role in achieving the antennas good performance while using a relatively simple mathematical model for this complex geometry. Furthermore, the developed mathematical model generates flare shapes that are very close to those found empirically in the prototypes like that in Figure 2 b-c.

Finally, the width of the flare measured with respect to its parametric length  $q$  that is originated from the feed point  $O^2$  can be defined by the following shaping function illustrated in Figure 5

$$W(q) = W_{\min} + \left[ \frac{q - L}{L} \right]^m (W_{\min} - W_{\max}) \quad (5)$$

where the quantities  $W_{\min}$  and  $W_{\max}$  define the minimum and maximum width for the flare, respectively; the power factor  $m$  shapes the flare edge;  $L$  is the maximum length of the tongue along its flat profile before it is bent.

## 4. Asymmetrical Two-Flare Antenna

### 4.1. Prototype Simulation and Design

A prototype of UWB antenna recently developed and tested in the UMass Antenna and Propagation Laboratory is shown in Figure 6 with a few samples of tongue flares in Figure 7. This antenna element is particularly designed to occupy a relatively compact physical space of the 7x8x3 cm overall size and operate in the band with lower frequency around 2 GHz. The upper frequency is defined by the size and construction of the feed region. The upper frequency limit is projected for this design to be approximately to 10 GHz.

For the given bandwidth, the antenna aperture size is about  $0.5\lambda$  size at the lower 2 GHz frequency,  $1.5\lambda$  at 6 Hz and  $2.5\lambda$  at 10 Hz. The expected performance includes: (1) a wide nearly 50- $\Omega$  impedance bandwidth and (2) 5-dBi directive gain with a nearly constant beam and  $>10$ dB front-to-back ratio. In particular, the operating band makes this antenna suitable for FCC unlicensed 3-10 GHz band.

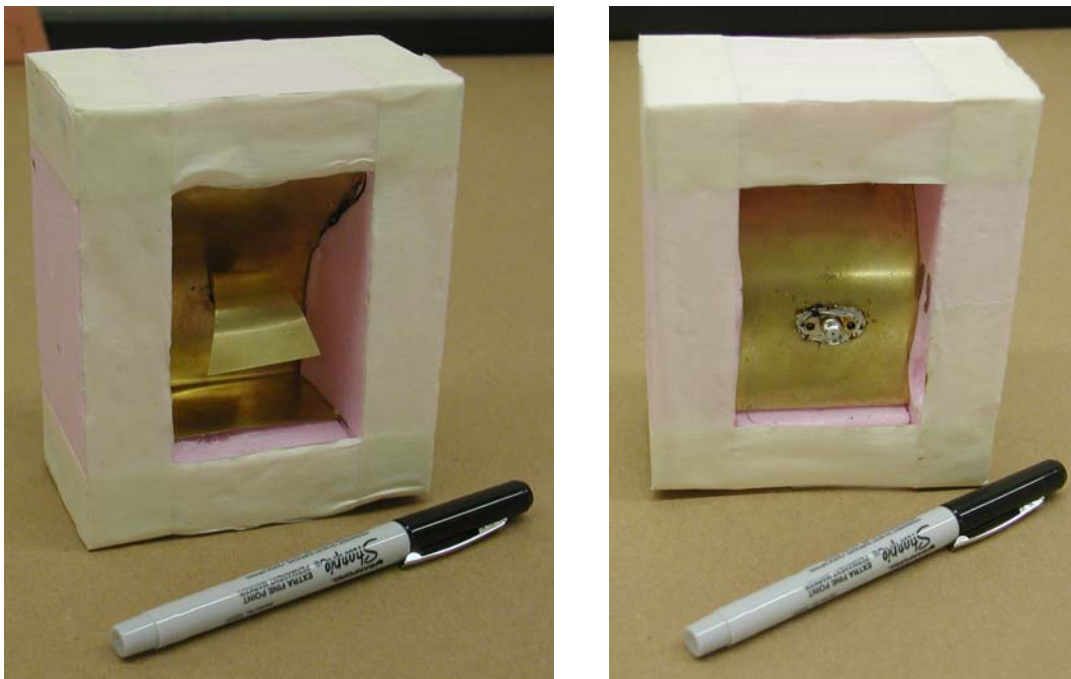


**Figure 6.** A compact prototype of UWB antenna operating in the 2-10 GHz band: (a) front view; (b) backside view with SMA coaxial connector. A foam support surrounds the antenna. In production, the reflector can be fabricated from self-supporting material, eliminating the need for external support.



**Figure 7.** A few samples of the tongue flare used in prototype in Figure 6. The elements are soldered to the central pin of the coaxial SMA connector.

Several full-wave simulation tools were used to predict the antenna performance and optimize its geometry including (1) a frequency-domain Method-of Moment (MoM) solver developed at UMass (MEMA = Massachusetts Electromagnetic Analyzer), (2) PB-FDTD (Periodic Boundary FDTD from Henrik Holter, Sweden) and (3) HFSS (Ansoft Inc.). The use of these diverse codes enables their mutual verification and increase confidence that predictions will match future measured results.

A set of geometrical and mesh models is used which are generated by a number of Matlab scripts and illustrated in Figure 8. In particular, three basic geometrical models are created for the flare profiles in Figure 8a that is algorithmically based on the mathematical results presented early in Section 3. The first model in Figure 8b contains a number of flat polygons used for generating all necessary meshes, viz. triangular-faceted MoM mesh, Figure 8c, and FDTD staircase mesh, Figure 8d. Additionally, the polygon model in Figure 8b is used for interfacing to CAD tools and HFSS simulation software using suitable graphical file standards, e.g. DXF, STL. Note: In practice, a finer mesh than those shown in Figure 8 b-d is required for computations to predict accurately the antenna electrical features.

#### **4.2. Antenna Optimization**

The antenna is optimized before prototyping by using the UMass MEMA MoM solver within a Matlab-based optimization code. The primary objective in optimization is supporting the “flat” nearly  $50\text{-}\Omega$  input resistance and nearly “zero” input reactance in the band of interest. No specific requirement is enforced for the antenna radiation features. Thus the observed antenna radiation features are just a “byproduct” of applying the above optimization procedure to the antenna port characteristics.

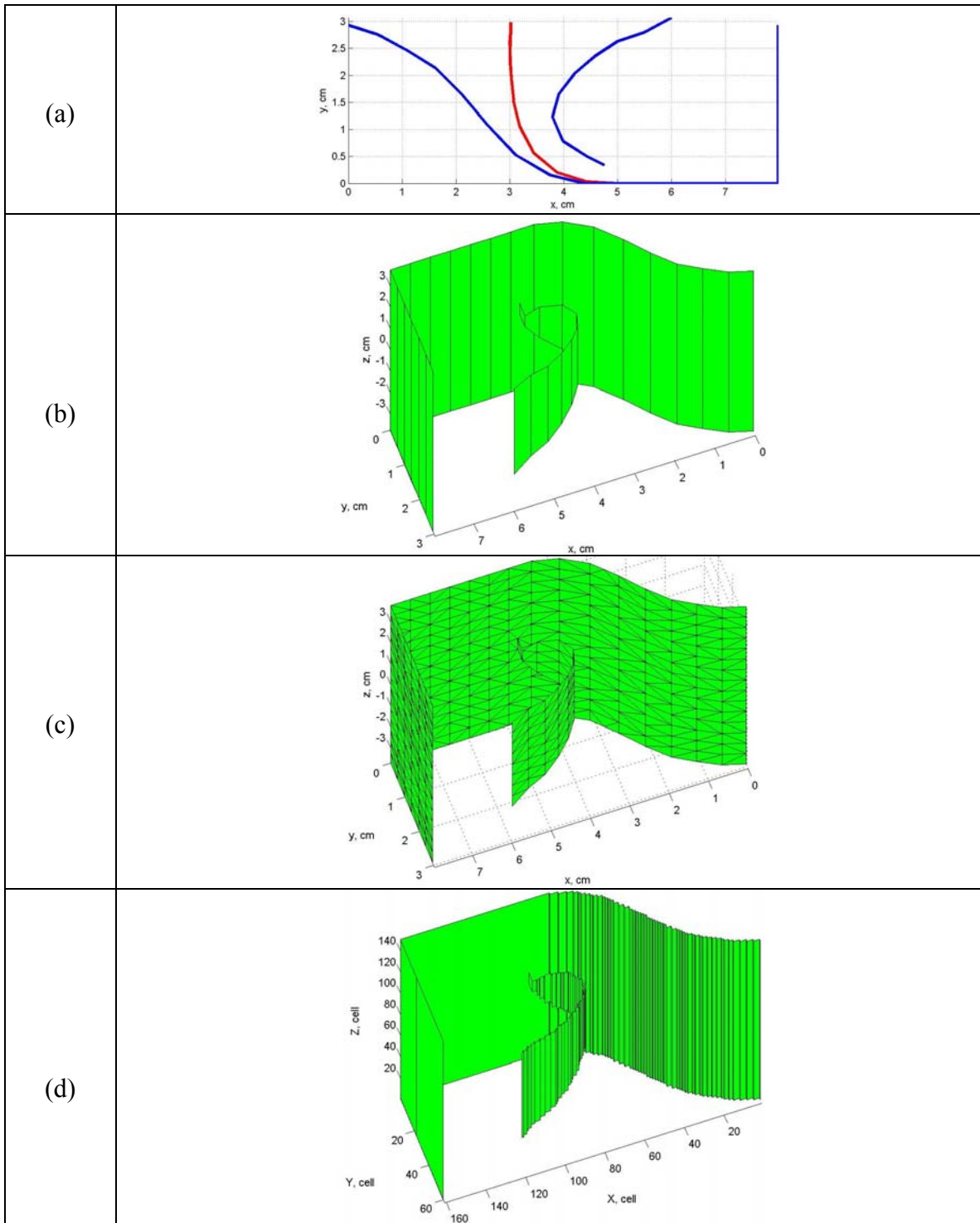


**Figure 8.** Geometrical model of the prototype in Figure 6: (a) shape flares; (b) CAD polygon model of flare surfaces, (c) MoM model mesh, (d) FDTD model staircase mesh (0.5 mm cell size).

The optimization parameters include the following geometrical features arranged in the order how strongly they affect on the 50- $\Omega$  impedance bandwidth:

1. The height of the flare # 2 over the flare # 1 at the feed point,  $H_F$ .
2. The shape parameter  $n$  for the base curve in equation (1).
- 3-5. The parameters  $W_{\min}$ ,  $W_{\max}$  and  $m$  to specify the flare #2 width in equation (5).
- 6-7. The parameters  $R_1^i$  and  $R_2^i$  for flare shaping in equations (2)-(3).

The design constraints involve the antenna overall size, viz. its aperture size and the antenna height, e.g. 7x8x3 cm as in Figure 6. The optimization procedure is based on linear golden-section search strategy in the multidimensional parametric space. Gradient-based searching methods are not used because they require hundreds of iteration steps while the developed technique needs typically 5-8 iterations per parameter. A Pade-based adaptive frequency sampling is introduced for fast frequency sweeping, allowing the whole band to be sweep in a few minutes per iteration.

### 4.3. Antenna Terminal Characteristics

The simulated and measured input impedance and VSWR are shown in Figures 9 and 10. The simulated data are obtained with MoM, FDTD and FEM (HFSS) EM simulation tools and computational models as described in conjunction with Figure 8. The antenna impedance bandwidth is affected at the lower frequencies by a single low-Q resonance compared to that in broadband dipole antennas. In fact, intensity of this resonance depends on a proper choice in the antenna geometry including the feed area geometry and tongue flare shape. After that resonance, the input resistance is typically a bit lowered to the level of about 30  $\Omega$  while the input reactance is capacitive. Afterwards, starting from the frequency about 4 GHz the input resistance is around 50  $\Omega$  while the input reactance is inductive. Totally, the antenna has an acceptable VSWR shown in Figure 10 for the simulated and measured data.

Some observable discrepancy exists between the simulated and measured data in Figures 9 and 10 that can be explained by a number of factors specific for each EM numerical tool. However, the most of the discrepancy comes from some dissimilarity of the antenna feed modeling, e.g. for MoM, Figure 11a, and FDTD, Figure 11b, compared to its real physical structure in Figure 11c. The HFSS solver is applied because of possibility to model accurately the antenna feeding coaxial line. However some other factors disturb the HFSS results around the first resonance while the HFSS simulated data are well agreed to other method data at the middle and upper part of the band. Neither MoM nor FDTD accurately predict the resistance and reactance peaks of the resonance, though they capture the basic phenomena fairly well. At the higher frequencies, FDTD simulated data are less accurate compared to those derived with MoM that are in closer agreement with measurements.

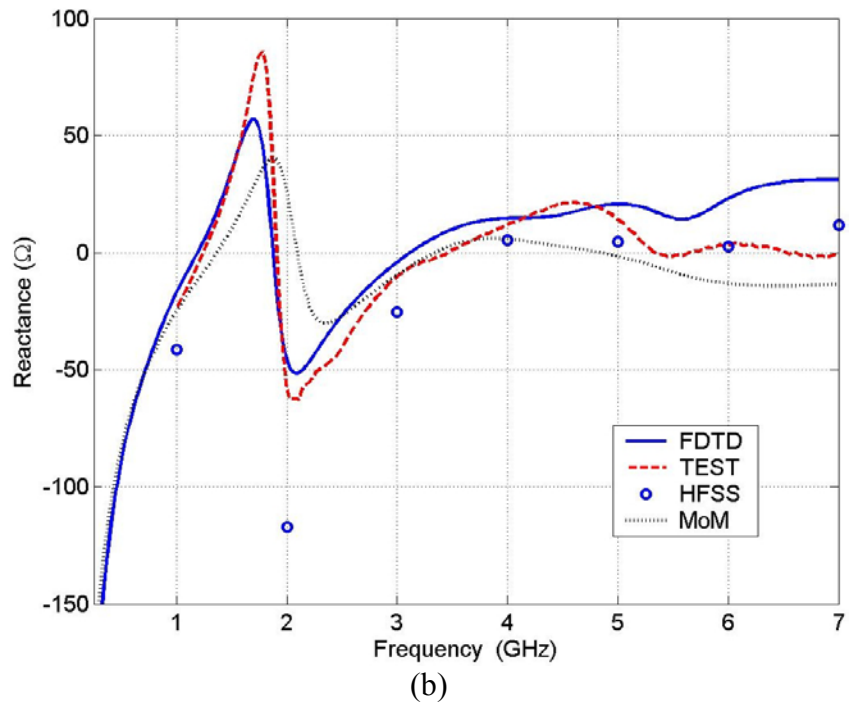
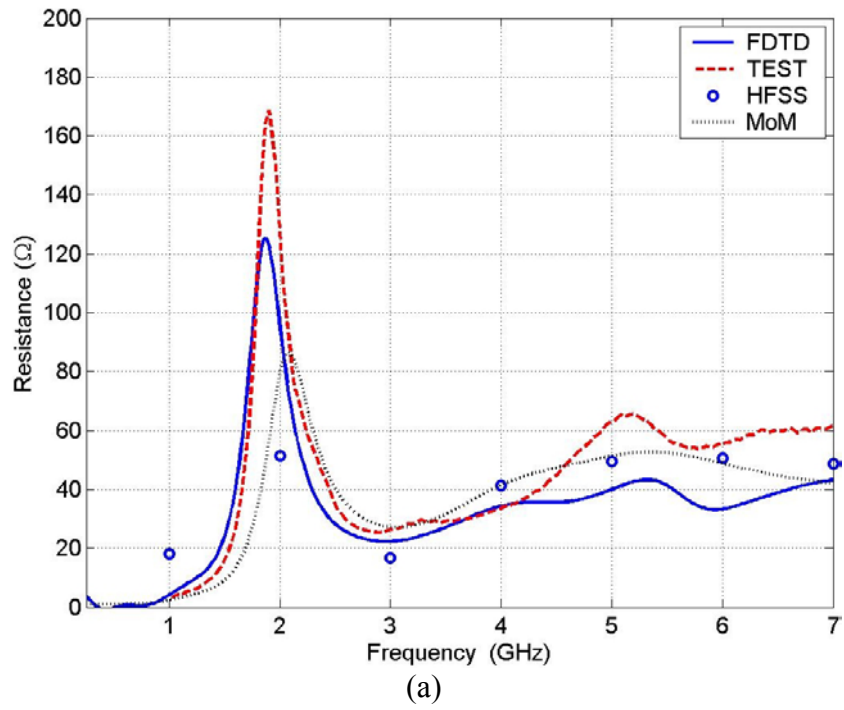


**Figure 9.** Predicted (FDTD, FEM-HFSS, MoM) and measured (TEST) input impedance of two flare antenna in Figure 6: (a) resistance and (b) reactance.

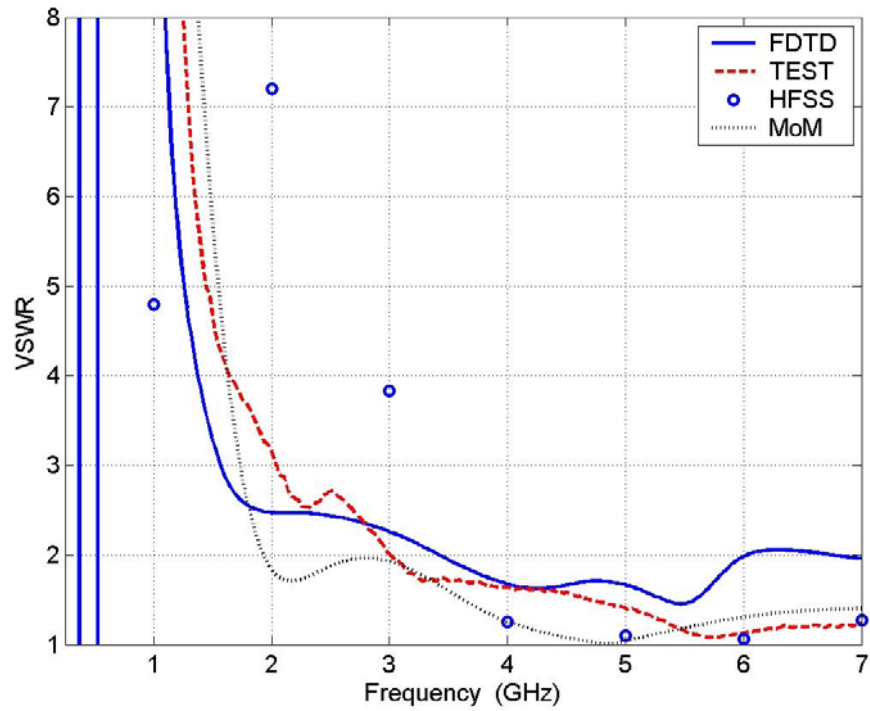


**Figure 10.** Predicted (FDTD, FEM-HFSS, MoM) and measured (TEST) VSWR of two-flare antenna in Figure 6.

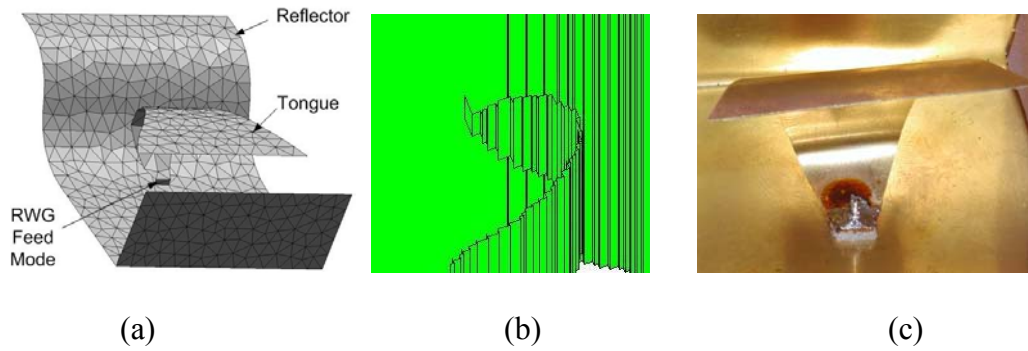


**Figure 11.** Configuration of the antenna feed: (a) for MoM simulation model; (b) FDTD simulation model; (c) actual feed soldered to the central pin of the SMA connector with a piece of supporting foam dielectric between the reflector and tongue.

#### **4.4. Antenna Radiation Characteristics**

This subsection demonstrates the radiation features of the antenna shown in Figure 6. The overall antenna size is 7 cm wide (H-plane) by 8 cm high (E-plane) by 3 cm deep. The MoM simulated and measured radiation patterns are plotted in Figure 12 for the E-plane and H-plane at the frequencies 3, 4, 5 & 6 GHz. An acceptable agreement is demonstrated in Figure 12 for the predicted and measured patterns. Most of the observable discrepancy is for the angular direction of 90° and further off broadside because of the impact of the antenna feed coaxial cable and other elements for antenna mounting in the chamber that are not included in the antenna numerical models.

The beam in the E-plane is slightly asymmetrical because of the antenna's asymmetrical geometry in the E-plane, Figure 2. At the same time, the antenna exhibits a good stability of the beam shape in broadband. In particular, the H-plane beam is nearly constant in the band and equals to about 120 degree at the level of -5 dB. The E-plane beam is a little variable but hold within 90 degree for the -5 dB reference level.

The antenna gain is nearly constant and equal to 5 dBi in the band. The front-to-back ratio is at least 10dB throughout the band. This figure can be further improved by using larger reflector flare but this design is primary concerned with a compact antenna structure. Simulated and measured cross-polarization components of the radiated fields are the level -30 dB and less in the principal plane.

#### **4.5. Surface Current Distribution**

The broadband characteristics of the proposed antenna can be partially understood by inspecting its current distribution. In particular, a tapered TEM transmission line section in the feed area, when it is properly designed, creates low-current standing wave ratios. A set of the predicted surface current distribution data is plotted in Figure 13 for the frequencies 2, 3, 4 & 6 GHz. The following salient features are observable for the simulated current distribution:

1. The current flows from the feed point like a traveling wave because it does not change the propagation direction and does not creates standing wave patterns.
2. The current is mostly spread (except the low frequencies) over the tongue flare and the nearby part of the reflector flare.
3. The current is relatively more distributed over the antenna surface at 2 GHz but does not vary much at the frequencies > 2 GHz.

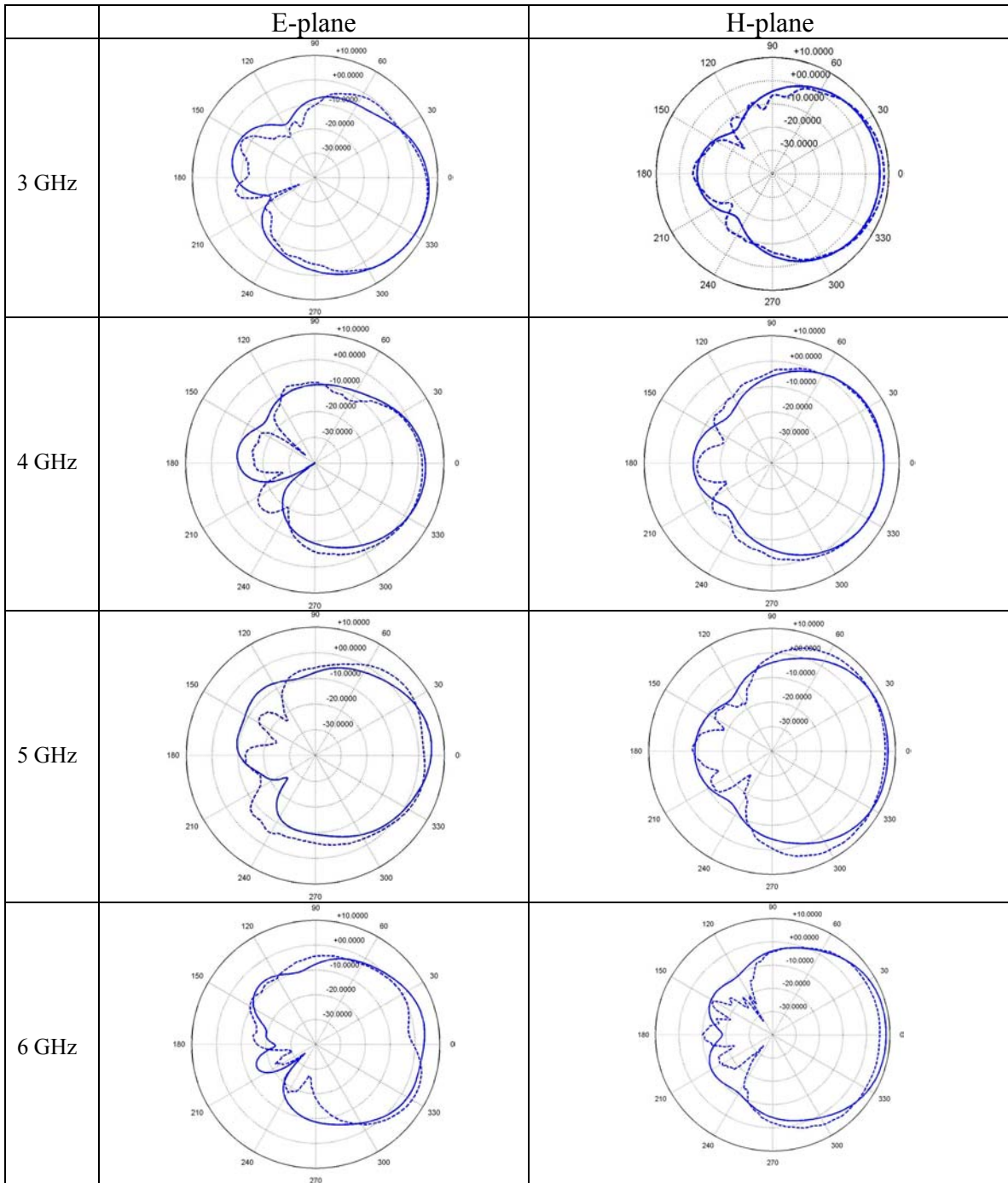


**Figure 12.** Simulated (solid) and measured (dash) radiation pattern in the E-plane (left) and H-plane (right) for the 3-6 GHz band.

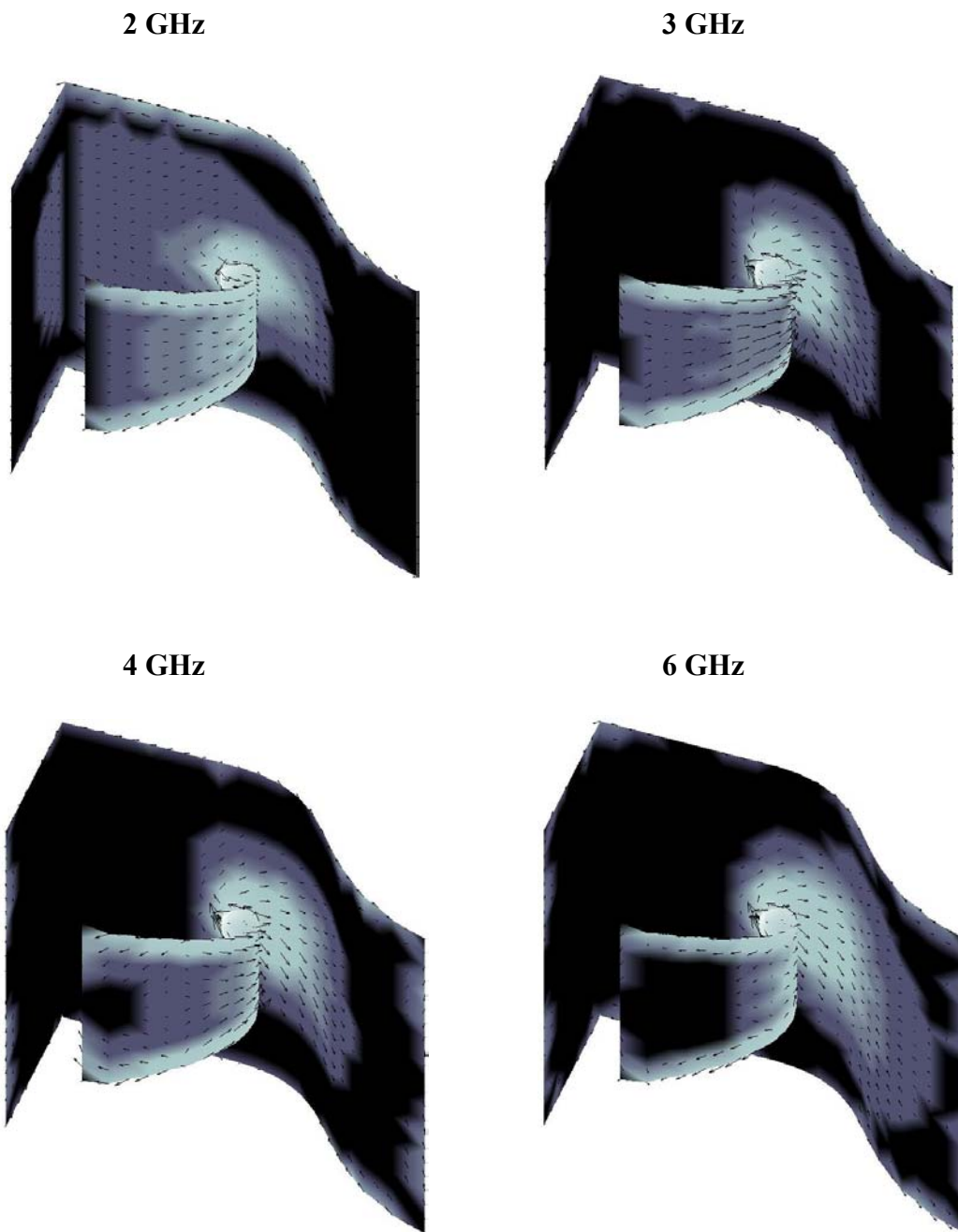


**Figure 13.** Simulated surface current distribution for several frequency points. Maximum of the surface current is marked by the bright spots while dark areas mean very low current intensity. Arrows show details of the surface current distribution for the bright spots.

#### 4.6. Antenna Signal Transmission Characteristics

Distortionless pulse signaling requires a short impulse response for the antenna or, equivalently, “flat” gain and “linear” phase responses in the frequency domain. To this end, a transmission characteristic is computed, Figure 14, relating the antenna port driving voltage to the principal radiated field component taken along broadside direction in the far-field.

The gain characteristic in Figure 14 is normalized by removing the free-space energy divergence and phase factor. The flatness of the gain in the 5:1 band with less than 2dB variations is an excellent feature of this antenna that means constant frequency-independent beam and constant directive gain, viz. about 5 dBi as discussed early. The phase characteristic is nicely linear that enables pulse signaling with very low distortions that is also experimentally confirmed for UWB radar using such antennas. Thus, this UWB antenna is usable for the FCC 3-10 GHz band.

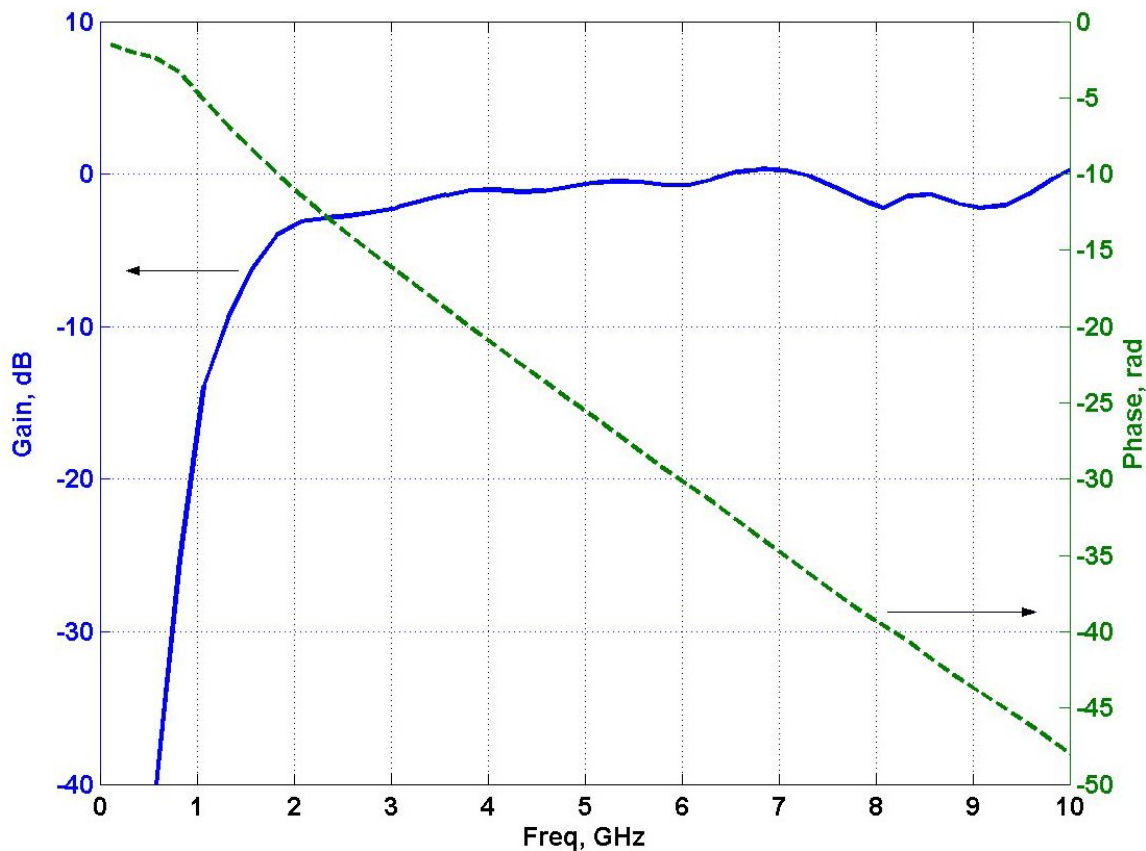


**Figure 14.** Antenna transmission characteristics for far-field principal field component (free space energy divergence is compensated).

## 5. Other Antenna Design Modifications

A number of other antennas of the novel design are tested including a variety of prototypes made in Kiev, Ukraine and the Antennas and Propagation Laboratory of UMass, USA. Another prototype made recently at UMass is shown in Figure 15. This antenna is larger than the one described in Section 4 and it has a doubly flared reflector (Figure 3a) instead of a vertical wall (Figure 2a). This new antenna size is 21x18x9 cm. However the antenna feed area is not directly scalable and requires special consideration. The enlarged antenna operates at the lower frequencies that are very important for applications related to through-matter (subsurface) UWB sensing. The symmetrical reflector flare leads to a more symmetrical radiation pattern in the E-plane.

The measured VSWR characteristic is illustrated in Figure 16 that shows antenna usability in the band of about 9:1. Some degradation at the frequencies  $> 8$  GHz is due to (1) the UHF connector limited in the band above approximately 7-8 GHz and (2) antenna feed should be adjusted for better performance.

In addition, this antenna has a tuning option via moving of the free end of the tongue flare as illustrated in Figure 15c. This end is held by a foam movable bar. It was found in some experiments with subsurface radars that this feature can be helpful in matching of UWB antennas that are disturbed by dielectric material media in close proximity to the antenna. An antenna similar to the one in Figure 15 is used in a three-element array of UWB through-wall radar vision system developed by the Ratio, Kiev, Ukraine and illustrated in Figure 17. The central element is used for transmitting and the outer two elements are used with two receivers forming a two-element receiving array.

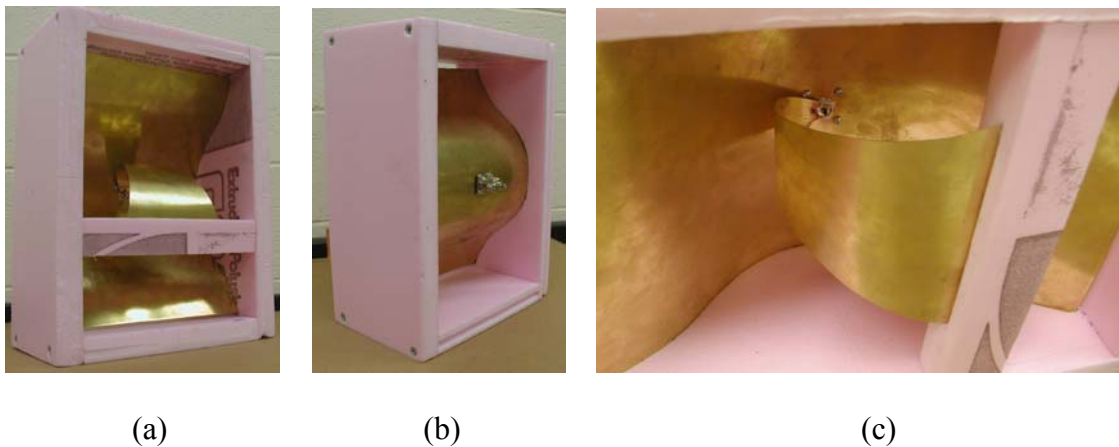


**Figure 15.** Enlarged two-flare antenna prototype: (a) front aperture view; (b) backside view with UHF coaxial connector; (c) some design details on tongue flare mounting.

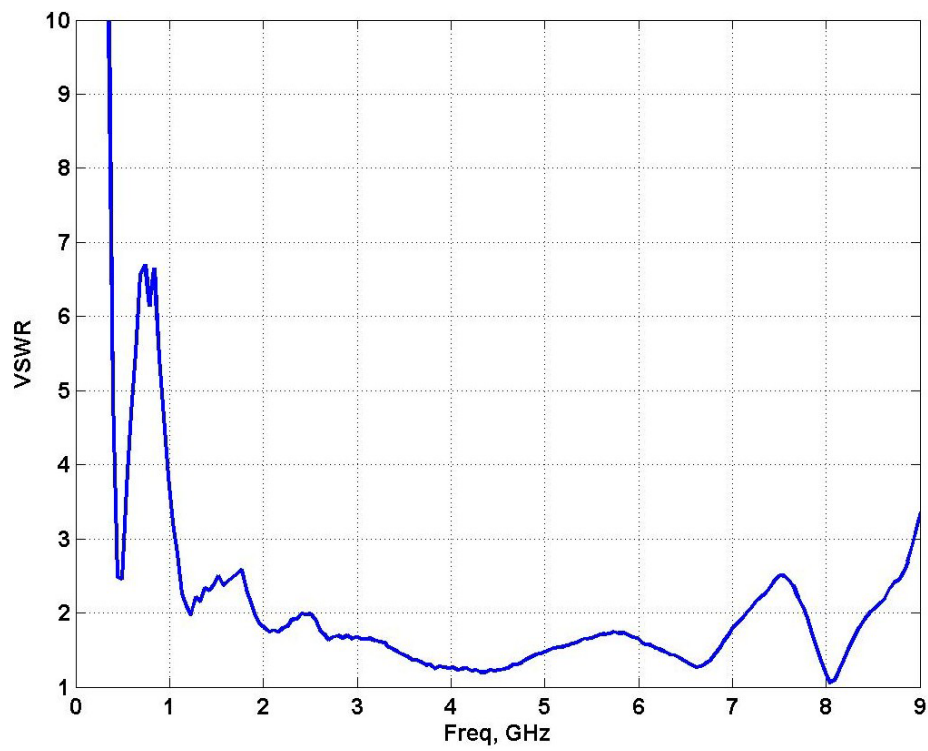
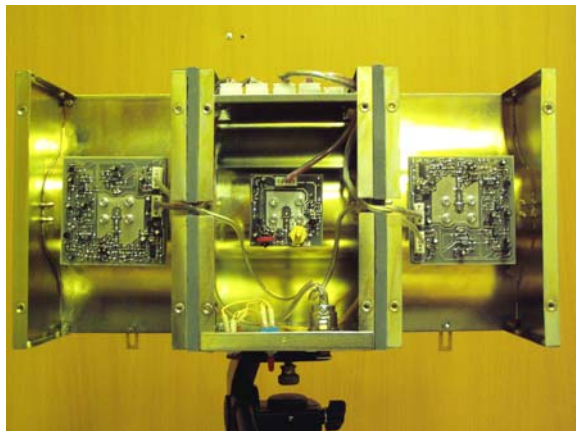


**Figure 16.** Measured VSWR for the antenna prototype in Figure 15.



(a)



(b)

**Figure 17.** An experimental UWB radar system with 3-element array of two-flare antennas: (a) front (aperture) view, (b) backside view with PCBs for receivers (at the left and right) and transmitter (at the middle).

## **6. Conclusions**

A novel design of a simple UWB directive antenna is presented and discussed. The antenna geometrical and EM numerical models are created. Its electrical performance is predicted with MoM, FDTD and FEM full-wave solvers. The antenna design is numerically optimized before prototyping to provide its desired electrical features, e.g. wideband  $50\text{-}\Omega$  impedance. Several prototypes of this antenna have been manufactured in house and their electrical terminal and radiation characteristics have been measured and discussed.

This design presents a relatively compact physical structure to operate in bandwidths around 5:1. In particular, this antenna demonstrates a frequency-independent behavior holding small variations for the input impedance and constant beamwidth as demonstrated for simulated and measured results. In general, the presented antenna exhibits an efficient use of the occupied physical space. The antenna prototype of the 7.5x6x3 cm size demonstrates beam stability and approximately 5 dBi gain with more than 10 dB front-to-back ratio.

Acceptable correspondence is obtained between numerically predicted and measured terminal and radiation characteristics. Some discrepancy exists between the numerical and measured results because very fine meshing is required to model properly the antenna 3-D complex shape including its feed area that is a critical part of the two-flare antenna design.

## **7. Acknowledgments**

This work is partially supported DoD MURI Grant DAAD 19-01-1-0477. The authors express their sincere gratitude the UMass students Matthew Carrier for providing antenna manufacturing and testing, Sreenivas Kasturi for his help with simulation using commercial software and Sergey Galatsuk from the Ratio Company, Kiev, Ukraine for his great contribution to make the first prototypes of the two-flare UWB antenna, and Prof. Daniel Schaubert for helpful discussions during the simulations and testing.

## 8. References

- [1] K. Siwiak, D. McKeown, *Ultra-Wideband Radio Technology*, Wiley, 2004.
- [2] D. Daniel, *Ground Penetrating Radar*, IEEE Publishing, 2004.
- [3] *Ultra-Wideband Radar Technology*, edited by J. D. Taylor, CRC Press, 2001.
- [4] A. H. Mohammadian, A. Rajkotia, S. S. Soliman, "Characterization of UWB Transmit-Receive Antenna System", *IEEE Conference on Ultra Wideband Systems and Technologies*, 2003, pp. 157 - 161.
- [5] W. Sorgel, W. Wiesbeck, "Influence of Antennas on the Ultra-Wideband Transmission", *EURASIP Journal Of Applied Signal Processing*, No. 3, 2005, pp. 296-305.
- [6] H.F. Harmuth, *Antennas and Waveguides for Nonsinusoidal Waves*, Academic Press, 1984.
- [7] H. G. Schantz, "Introduction to Ultra-Wideband Antennas", *IEEE Conference on Ultra Wideband Systems and Technologies*, 2003, pp. 1-9.
- [8] R. C. Johnson, *Antenna Engineering Handbook*, McGraw-Hill, 3<sup>rd</sup> ed.
- [9] K.Y. Lai, A. L. Sinipoli and W. D. Burnside, "A novel antenna for ultra-wideband applications," *IEEE Transactions on Antennas and Propagation*, Vol. 40, July 1992, pp. 755-760.
- [10] P. Eskelinen, "Improvements of a Trapezoidal Pulse Antenna," *IEEE Antennas and Propagation Magazine*, Vol.43, June 2001, pp.82-85.
- [11] C. E. Baum, E.G. Farr, "Impulsive Radiating Antennas", in *Ultra-Wideband Short-Pulse Electromagnetics*, Plenum Publisher, 1993, pp. 139-147.
- [12] K.-L. Wong, *Compact and Broadband Microstrip Antenna*, John Wiley & Sons, Inc., 2002.
- [13] G. Kumar, K. P. Ray, *Broadband Microstrip Antennas*, Artech House, Boston, 2003.
- [14] Sostanovsky D.L, Boryssenko A.O, "A Novel Tongue UWB Antenna", *Patent Ukraine #65488 A*, Filed November 28, 2003, Issued March 3, 2004, Bulletin #3.
- [15] D. F. Rogers, *An Introduction to NURBS with Historical Perspective*, Morgan Kaufmann Publishers, 2001.
- [16] J. Shin, D. H. Schaubert, "A Parametric Study of Stripline-Fed Vivaldi Notch-Antenna Arrays", *IEEE Transaction on Antennas and Propagation*, Vol. 47, No. 5, May 1999, pp. 879-866.